# *$[Ba_4Cl_2][HgGa_4S_{10}]$: Modulating covalency and ionicity in Hg-based material achieving strong second harmonic generation response and wide band gap*

Yujie Zhang,† Hongping Wu,† Zhanggui Hu,† Jiyang Wang,† Yicheng Wu,†and Hongwei Yu,*,†

†*College of Functional Crystals, Tianjin University of Technology, No.391 Bin Shui Xi Dao Road, Xiqing District, Tianjin 300384, China*

To whom correspondence should be addressed. E-mail: hwyu15@gmail.com (Hongwei Yu).

**CONTENTS**

**Experimental Section**

**Synthesis**. Ba (99.9%), $Ga_2S_3$ (99.9%), HgS (99%), $BaCl_2$ (99.5%), and S (99.9%) were purchased from Beijing Hawk Science and Technology Co. Ltd. (China), all the reagents were commercially purchased without further refinement. For the preparation of $[Ba_4Cl_2][HgGa_4S_{10}]$, reactants of Ba (3 mmol), $Ga_2S_3$ (2 mmol), HgS (1 mmol), $BaCl_2$ (1.5 mmol), S (3.5 mmol) were firstly loaded into a graphite crucible and then they are sealed into the silica tube and flame-sealed under $10^{-3}$ Toor. The tube was placed in a temperature-controlled furnace with the following heating process: firstly, the temperature was raised to 750 °C at a rate of 5 °C/h and kept at this temperature for 100 h. Subsequently, the furnace was slowly cooled down to 300 °C at a rate of 3 °C/h. Finally, the furnace was turned off and cooled down to room temperature. N, N−dimethylformamide (DMF) solvent was chosen to wash the products. Finally, many millimeter-level pale-yellow crystals of $[Ba_4Cl_2][HgGa_4S_{10}]$ were obtained with yields of ∼80%, and all of them are stable under air and moisture conditions for at least 3 months.

**Crystal structure determination**. Powder X-ray diffraction (PXRD) pattern was collected setting from the 2θ range 10-70° with a step width size of 0.01° and a step time of 2 s on an automated SmartLab 3KW powder X-ray diffractometer using Cu-$K_\alpha$ radiation ($\lambda$ = 1.54057 Å) radiation. The purity of compound $[Ba_4Cl_2][HgGa_4S_{10}]$ was verified by PXRD with the results as shown in Figure S1 (Supporting Information online). The crystal structure of $[Ba_4Cl_2][HgGa_4S_{10}]$ was determined by single-crystal XRD on a Bruker SMART APEX III CCD diffractometer using Mo $K_\alpha$ radiation ($\lambda$ = 0.71073 Å) at 296(2) K and the data was integrated with the SAINT program.[1] All calculations were implemented with programs from the SHELXTL crystallographic software package.[2] Their crystal structures were solved by direct methods using SHELXS and refined with full-matrix least-squares methods on $F^2$ with anisotropic thermal parameters for all atoms.[3] Crystal data and structure refinement parameters were given in Table S1 (Supporting Information online). Some structural parameters including interatomic distances and angles, final refined atomic positions and isotropic thermal parameters are listed in Table S2 and Table S3, respectively.

**Energy-Dispersive Spectroscopy.** Microprobe elemental analyses and the elemental distribution maps were measured on a field-emission scanning electron microscope (Quanta FEG 250) made by FEI.

**UV−Vis−NIR Diffuse reflectance**. The UV−Vis−NIR optical diffuse reflectance spectrum of $[Ba_4Cl_2][HgGa_4S_{10}]$ in the range of 200−2500 nm was measured on Shimadzu SolidSpec-3700DUV with $BaSO_4$ as a reference. The band gap was estimated on basis of the absorption spectrum that was derived from the reflection spectrum using the Kubelka-Munk formula.[4]

**IR and Raman spectroscopy**. The IR spectrum was measured on a Nicolet iS50 Fourier transform IR spectrometer with ATR in the range of 4000−400 $cm^{-1}$. The Raman spectrum of

$[Ba_4Cl_2][HgGa_4S_{10}]$ in the range of 1000−10 $cm^{-1}$ was recorded on WITec alpha300R.

**Second-harmonic generation measurement**. The SHG signals of $[Ba_4Cl_2][HgGa_4S_{10}]$ and benchmark AGS were investigated under incident laser radiation of 2090 nm by modified Kurtz-Perry method, respectively.[5] Samples $[Ba_4Cl_2][HgGa_4S_{10}]$ and AGS were sieved into several distinct particle size ranges (54−75, 75−100, 100−125, 125−150, 150−180, and 180−250 μm) for the PM measurements. The SHG signals were detected by a charge-coupled device. The second harmonic efficiency of the $[Ba_4Cl_2][HgGa_4S_{10}]$ powder was compared to that of AGS powder with the same particle size.

**Laser damage threshold measurement**. The LDTs of the $[Ba_4Cl_2][HgGa_4S_{10}]$ and AGS powder at the particle size range of 100−125 μm were evaluated under using high-power laser irradiation of 1064 nm (pulse width $\tau_p$ = 10 ns) by the single-pulse method.[6] The measurement processes were performed by gradually increasing the laser power until the damaged spot was observed under a microscope. The damage thresholds were derived from the equation $I_{(threshold)} = E/(\pi r^2 \tau_p)$, where $E$ is the laser energy of a single pulse, $r$ is the spot radius, and $\tau_p$ is the pulse width.

**Computational Methods**. The electronic band structures, the partial density of states, optical properties, overlap populations, and electron localization function (ELF) for $[Ba_4Cl_2][HgGa_4S_{10}]$ were carried out using the CASTEP package based on density functional theory (DFT).[7, 8] Generalized gradient approximation (GGA) parametrized by Perdew-Burke-Ernzerhof (PBE) functional was chosen for the exchange-correlation energy, and the pseudopotential was set as norm-conserving pseudopotential (NCP).[9] The valence electrons were set as: Ba $4d^{10}5p^66s^2$, Hg $5d^{10}6s^2$, Ga $4s^24p^1$, S $3s^23p^4$, and Cl $3s^23p^5$. The plane-wave energy cutoff value was set at 860.0 eV. The numerical integration of the Brillouin zone was performed using 4 × 4 × 2 Monkhorst-Pack $\kappa$-point meshes.[10]

The SHG coefficients were calculated from the band wave functions using the so-called length-gauge formalism derived by Aversa and Sipe at a zero-frequency limit. The static second-order nonlinear susceptibilities $\chi_{\alpha\beta\gamma}^{(2)}$ can be reduced as:[11, 12]

$$\chi_{\alpha\beta\gamma}^{(2)} = \chi_{\alpha\beta\gamma}^{(2)}(\mathrm{VE}) + \chi_{\alpha\beta\gamma}^{(2)}(\mathrm{VH}) \qquad (1),$$

Virtual-Hole (VH), Virtual-Electron (VE) and Two-Band (TB) processes play an important role in the total SHG coefficient $\chi^{(2)}$. The TB process can be neglected owing to little contribution for SHG. The formulas for calculating $\chi_{\alpha\beta\gamma}^{(2)}$ (VE) and $\chi_{\alpha\beta\gamma}^{(2)}$ (VH) are as follows:

$$\chi_{\alpha\beta\gamma}^{(2)}\ (\mathrm{VE}) = \frac{e^3}{2\hbar^2 m^3}\sum_{vcc'}\int\frac{d^3k}{4\pi^3}p(\alpha\beta\gamma)Im[P_{vc}^{\alpha}P_{cc'}^{\beta}P_{c'v}^{\gamma}]\left(\frac{1}{\omega_{cv}^{3}\omega_{vc'}^{2}}+\frac{2}{\omega_{vc}^{4}\omega_{c'v}}\right) \quad (2),$$

$$\chi_{\alpha\beta\gamma}^{(2)}\ (\mathrm{VH}) = \frac{e^3}{2\hbar^2 m^3}\sum_{vv'c}\int\frac{d^3k}{4\pi^3}p(\alpha\beta\gamma)Im[P_{vv'}^{\alpha}P_{v'c}^{\beta}P_{cv}^{\gamma}]\left(\frac{1}{\omega_{cv}^{3}\omega_{v'c}^{2}}+\frac{2}{\omega_{vc}^{4}\omega_{cv'}}\right) \quad (3),$$

Here, α, β, γ are Cartesian components, $v$ and $v'$ denote valence bands, $c$ and $c'$ refer to conduction bands, and $P(\alpha\beta\gamma)$ denotes the full permutation. The band energy difference and momentum matrix elements are denoted as $\hbar\omega_{ij}$ and $P_{ij}^{\alpha}$, respectively. As we know, the virtual electron (VE) progresses of occupied and unoccupied states are the main contribution to the overall SHG effect.[13]

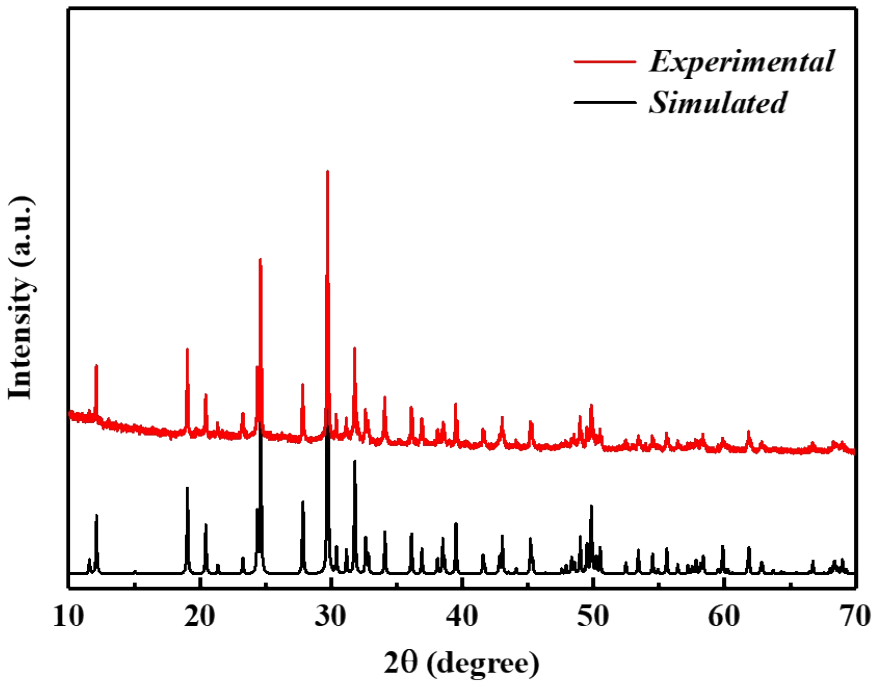


**Figure S1.** Experimental and calculated XRD patterns for $[Ba_4Cl_2][HgGa_4S_{10}]$.

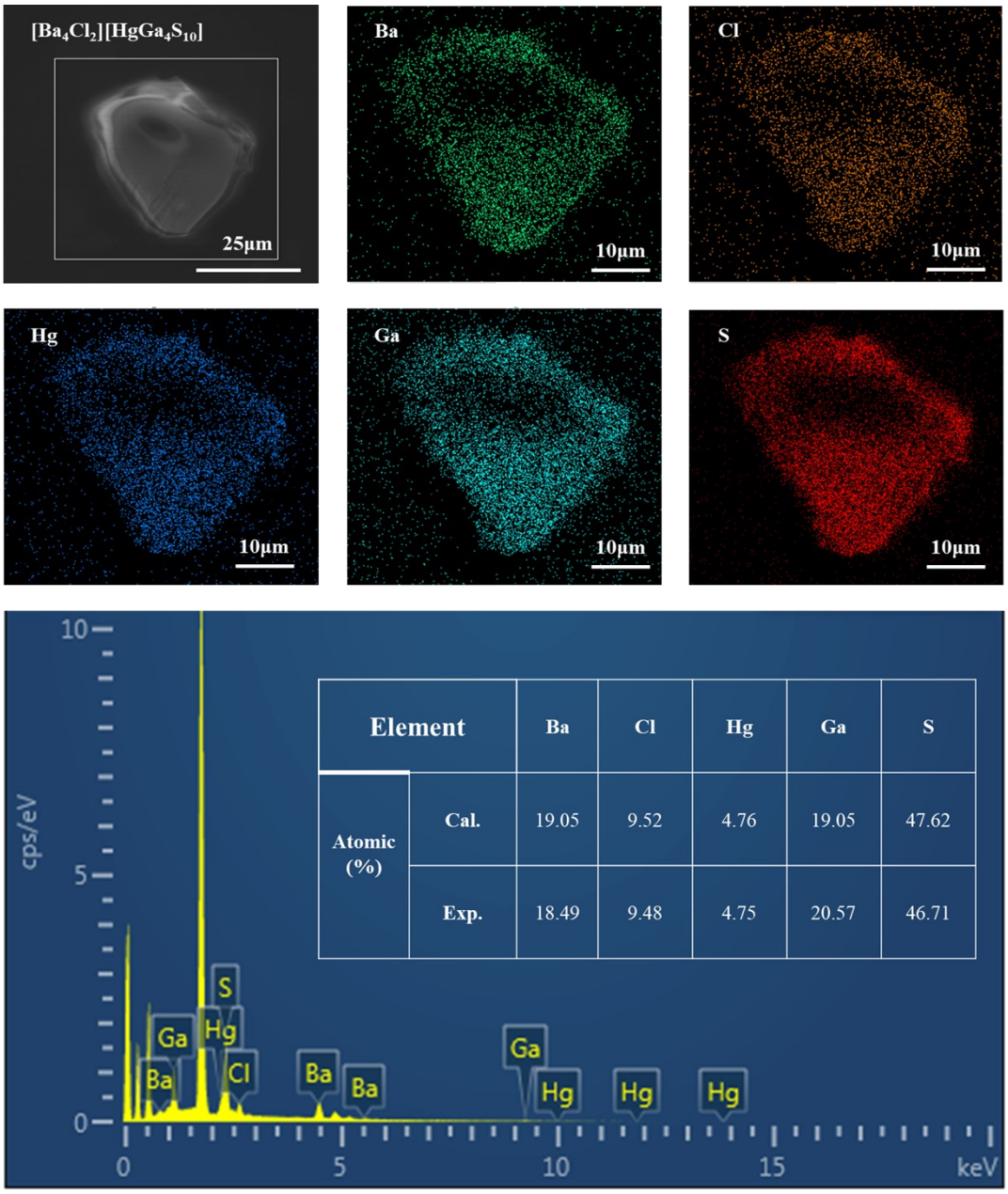


| Element | | Ba | Cl | Hg | Ga | S |
|---|---|---|---|---|---|---|
| Atomic (%) | Cal. | 19.05 | 9.52 | 4.76 | 19.05 | 47.62 |
| | Exp. | 18.49 | 9.48 | 4.75 | 20.57 | 46.71 |

**Figure S2.** EDS of $[Ba_4Cl_2][HgGa_4S_{10}]$.

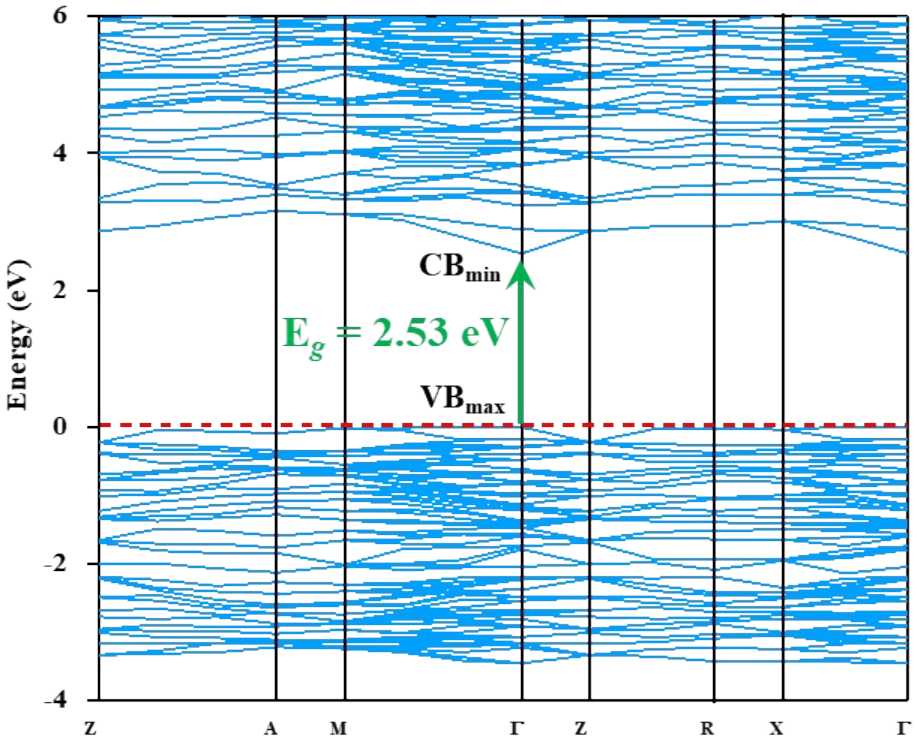


**Figure S3.** Calculated band structure of $[Ba_4Cl_2][HgGa_4S_{10}]$.

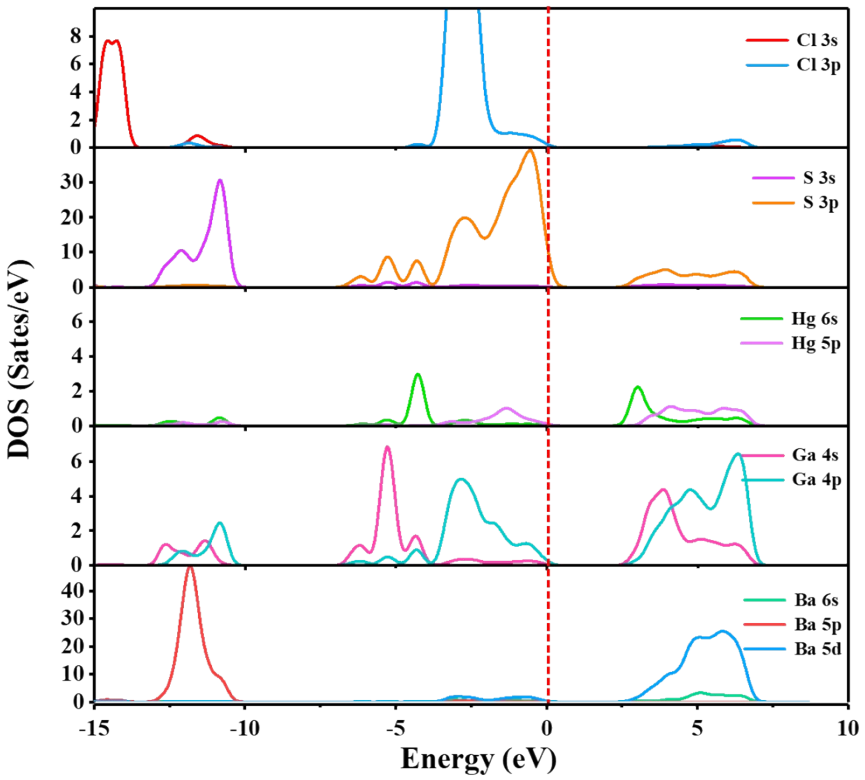


**Figure S4.** Projected density of states of $[Ba_4Cl_2][HgGa_4S_{10}]$

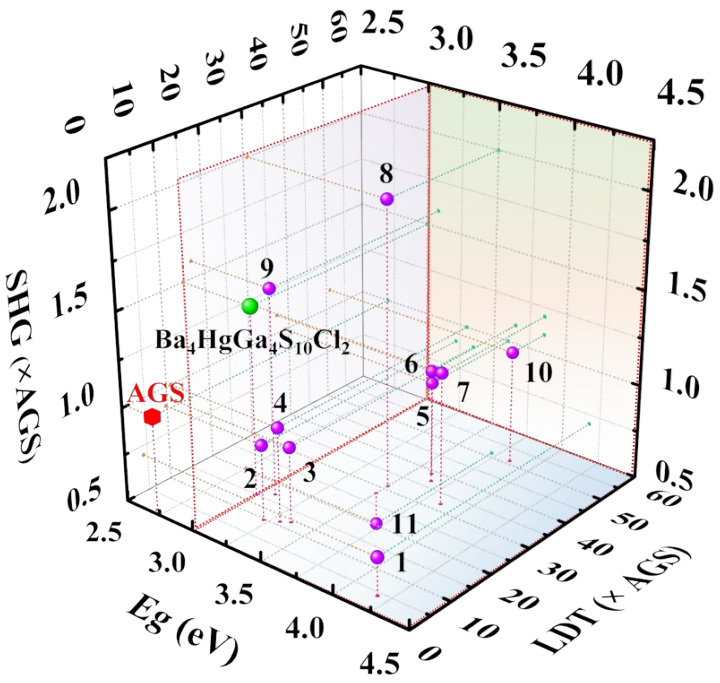


**Figure S5.** Three-dimensional diagram presenting the balanced performance of the LDT, SHG response, and band gap for chalcohalides.

**Table S1**. Local dipole moments for the [$GaS_4$], [$HgS_4$] and [$GaSe_4$] tetrahedra within a unit cell for [$Ba_4Cl_2$][$HgGa_4S_{10}$], [$Ba_4Cl_2$][$ZnGa_4S_{10}$], [$RbBa_2Cl$][$Ga_4S_8$], [$Ba_4Cl_2$][$ZnGa_4Se_{10}$], [$Ba_4Cl_2$][$CdGa_4Se_{10}$], and [$CsBa_3Cl_2$][$Ga_5Se_{10}$].

| Compounds | Tetrahedra | *Bonds* | *a* | *b* | *c* | *debye* |
|---|---|---|---|---|---|---|
| [$Ba_4Cl_2$][$HgGa_4S_{10}$] | $GaS_4$ tetrahedron | Ga-S | 0.38 | 2.29 | -1.89 | 2.99 |
| | $HgS_4$ tetrahedron | Hg-S | 0.0 | 0.0 | 0.0 | 0 |
| [$Ba_4Cl_2$][$ZnGa_4S_{10}$] | $GaS_4$ tetrahedron | Ga-S | 0.26 | 2.25 | 1.83 | 2.91 |
| [$RbBa_2Cl$][$Ga_4S_8$] | $GaS_4$ tetrahedron | Ga-S | 1.02 | 1.32 | 0.98 | 1.93 |
| [$Ba_4Cl_2$][$ZnGa_4Se_{10}$] | $GaSe_4$ tetrahedron | Ga-Se | -0.14 | 1.68 | -1.76 | 2.44 |
| [$Ba_4Cl_2$][$CdGa_4Se_{10}$] | $GaSe_4$ tetrahedron | Ga-Se | -0.22 | 1.61 | -1.73 | 2.37 |
| [$CsBa_3Cl_2$][$Ga_5Se_{10}$] | $GaSe_4$ tetrahedron | Ga-Se | 0.19 | -1.64 | 1.42 | 2.17 |

**Table S2**. Comparisons of $[Ba_4Cl_2][HgGa_4S_{10}]$ with other chalcohalides NLO materials on the Band gap, Laser-induced damage threshold, and SHG responses.

| Compound | Space group | Band gap (eV) | Laser-induced damage threshold (× AGS, MW/cm$^2$) | $d_{ij}$ (× AGS, pm/V) |
|---|---|---|---|---|
| 1. $Li[LiCs_2Cl][Ga_3S_6]$[15] | $Pna2_1$ | 4.18 | 4.1 | 0.7 |
| 2. $[KBa_3Cl_2][Ga_5Se_{10}]$[16, 17] | *I(-)*4 | 3.25 | 9.7 | 0.9 |
| 3. $[RbBa_3Cl_2][Ga_5S_{10}]$[18] | $Pmn2_1$ | 3.30 | 11.0 | 1.0 |
| 4. $[CsBa_3Cl_2][Ga_5S_{10}]$[18] | $Pmn2_1$ | 3.35 | 12.0 | 0.9 |
| 5. $[K_3Cl][Ga_3PS_8]$[19] | $Pmn2_1$ | 3.60 | 39.0 | 1.0 |
| 6. $[Rb_3Cl][Ga_3PS_8]$[19] | $Pmn2_1$ | 3.65 | 37.0 | 1.1 |
| 7. $[K_3Br][Ga_3PS_8]$[19] | *Pm* | 3.85 | 32.0 | 1.2 |
| 8. $[Rb_3Br][Ga_3PS_8]$[19] | *Pm* | 3.50 | 31.0 | 2.0 |
| 9. $[Ba_4Cl_2][ZnGa_4Se_{10}]$[17] | *I(-)*4 | 3.08 | 17.0 | 1.6 |
| 10. $[Ba_4Cl_2][ZnGa_4S_{10}]$[20] | *I(-)*4 | 3.85 | 51.0 | 1.1 |
| 11. $NaBa_4Ge_3S_{10}Cl$[21] | $P6_3$ | 3.49 | 20.0 | 0.33 |
| 12. $AgGaS_2$[14] | *I(-)*42*d* | 2.7 | 20.33 MW/cm$^2$ | 2.73 pm/V |
| 13. $[Ba_4Cl_2][HgGa_4S_{10}]$ | *I(-)*4 | 2.95 | 15.0 | 1.5 |

**Table S3.** Crystallographic Data and Refinement Details for $[Ba_4Cl_2][HgGa_4S_{10}]$.

| Empirical formula | $[Ba_4Cl_2][HgGa_4S_{10}]$ |
|---|---|
| Formula weight | 1420.33 |
| Temperature (K) | 296(2) |
| Crystal system | tetragonal |
| Space group | *I* (no.82) |
| Z | 2 |
| *a* (Å) | 8.308 (2) |
| *c* (Å) | 15.272 (4) |
| *V* (Å$^3$) | 1054.0 (7) |
| $D_c$ (g cm$^{-3}$) | 4.475 |
| $\mu$ (mm$^{-1}$) | 20.849 |
| *F*(000) | 1244 |
| Crystal size | 0.054 x 0.051 x 0.049 mm$^3$ |
| Radiation | Mo-$K_\alpha$ ($\lambda$ = 0.71073) |
| 2$\theta$ range(°) | 2.67 to 27.08 |
| Reflections collected | 2457 |
| Indep. Reflns/ Rint | 1158/0.0565 |
| GOOF on $F^2$ | 0.982 |
| $R_1$, $wR_2$ (I >2$\sigma$(I))[a] | 0.0416, 0.0783 |
| $R_1$, $wR_2$ (all data) | 0.0495, 0.0830 |
| largest diff. peak and hole (e·Å$^{-3}$) | 1.104, -1.403 |

[a] $R_1 = \Sigma||F_o|—|F_c||/\Sigma|F_o|$, [b] $wR_2 = \Sigma w(F_o^2—F_c^2)^2/\Sigma w(F_o^2)^2]^{1/2}$.

**Table S4.** Atomic coordinates ( × $10^4$) and equivalent isotropic displacement parameters (Å$^2$ × $10^3$) for $[Ba_4Cl_2][HgGa_4S_{10}]$. $U_{eq}$ is defined as one-third of the trace of the orthogonalized $U_{ij}$ tensor.

| Atom | BVS[a] | *Wyckoff* | *x* | *y* | *z* | $U_{eq}$(Å) |
|---|---|---|---|---|---|---|
| Ba(1) | 1.93 | 8*g* | 6443.2(2) | 2697.1(2) | 6397.9(1) | 0.023(1) |
| Hg(1) | 2.16 | 2c | 5000.0 | 0.0 | 2500.0 | 0.024(1) |
| Ga(1) | 3.07 | 8g | 8117.0(3) | 1106.0(3) | 4161.1(1) | 0.013(1) |
| S(1) | 1.80 | 8g | 10000.0 | 0.0 | 3270.0(4) | 0.023(2) |
| S(2) | 2.07 | 8g | 6406.0(6) | 2352.0(6) | 3249.0(3) | 0.017(1) |
| S(3) | 1.95 | 4*e* | 9265.0(6) | 3122.0(6) | 4949.0(3) | 0.016(1) |
| Cl(1) | 1.52 | 2b | 5000.0 | 0.0 | 7500.0 | 0.018(2) |
| Cl(2) | 1.30 | 2d | 5000.0 | 5000.0 | 5000.0 | 0.020(2) |

[a]Bond valence state was calculated using the empirical formula $V_i=\Sigma S_{ij}=\Sigma\exp[(r_0-r_{ij})/0.37]$, where $S_{ij}$ is the bond valence associated with bond lengths $r_{ij}$ and $r_0$.[22]

**Table S5.** Selected distances (Å) and angles (degrees) for $[Ba_4Cl_2][HgGa_4S_{10}]$.

| | | | |
|---|---|---|---|
| Ba(1)-Cl(1) | 3.0481(13) | S(3)-Ba(1)-S(2)#3 | 141.20(11) |
| Ba(1)-Cl(2) | 3.1073(13) | S(2)#1-Ba(1)-S(2)#3 | 94.03(12) |
| Ba(1)-S(3) | 3.243(5) | S(2)#2-Ba(1)-S(2)#3 | 112.89(9) |
| Ba(1)-S(2)#1 | 3.284(6) | Cl(1)-Ba(1)-S(3)#4 | 76.62(8) |
| Ba(1)-S(2)#2 | 3.345(5) | Cl(2)-Ba(1)-S(3)#4 | 97.84(8) |
| Ba(1)-S(2)#3 | 3.521(5) | S(3)-Ba(1)-S(3)#4 | 67.46(14) |
| Ba(1)-S(3)#4 | 3.534(5) | S(2)#1-Ba(1)-S(3)#4 | 145.21(12) |
| Ba(1)-S(1)#5 | 3.644(5) | S(2)#2-Ba(1)-S(3)#4 | 115.30(12) |
| Hg(1)-S(2)#8 | 2.548(5) | S(2)#3-Ba(1)-S(3)#4 | 111.02(12) |
| Hg(1)-S(2)#9 | 2.548(5) | Cl(1)-Ba(1)-S(1)#5 | 79.82(5) |
| Hg(1)-S(2)#10 | 2.548(5) | Cl(2)-Ba(1)-S(1)#5 | 95.11(7) |
| Hg(1)-S(2) | 2.548(5) | S(3)-Ba(1)-S(1)#5 | 135.75(9) |
| Ga(1)-S(2) | 2.244(5) | S(2)#1-Ba(1)-S(1)#5 | 58.58(8) |
| Ga(1)-S(1) | 2.267(4) | S(2)#2-Ba(1)-S(1)#5 | 61.25(10) |
| Ga(1)-S(3) | 2.272(5) | S(2)#3-Ba(1)-S(1)#5 | 56.70(8) |
| Ga(1)-S(3)#4 | 2.290(5) | S(3)#4-Ba(1)-S(1)#5 | 156.07(9) |
| Cl(1)-Ba(1)-Cl(2) | 132.86(5) | S(2)#8-Hg(1)-S(2)#9 | 101.63(8) |
| Cl(1)-Ba(1)-S(3) | 137.82(10) | S(2)#8-Hg(1)-S(2)#10 | 101.63(8) |
| Cl(2)-Ba(1)-S(3) | 75.12(9) | S(2)#9-Hg(1)-S(2)#10 | 126.65(19) |
| Cl(1)-Ba(1)-S(2)#1 | 135.96(8) | S(2)#8-Hg(1)-S(2) | 126.65(19) |
| Cl(2)-Ba(1)-S(2)#1 | 69.68(8) | S(2)#9-Hg(1)-S(2) | 101.63(8) |
| S(3)-Ba(1)-S(2)#1 | 77.86(12) | S(2)#10-Hg(1)-S(2) | 101.63(8) |
| Cl(1)-Ba(1)-S(2)#2 | 74.60(9) | S(2)-Ga(1)-S(1) | 104.58(18) |
| Cl(2)-Ba(1)-S(2)#2 | 142.60(10) | S(2)-Ga(1)-S(3) | 104.76(19) |
| S(3)-Ba(1)-S(2)#2 | 101.06(12) | S(1)-Ga(1)-S(3) | 109.06(17) |
| S(2)#1-Ba(1)-S(2)#2 | 73.13(15) | S(2)-Ga(1)-S(3)#4 | 113.1(2) |
| Cl(1)-Ba(1)-S(2)#3 | 72.02(9) | S(1)-Ga(1)-S(3)#4 | 113.30(16) |
| Cl(2)-Ba(1)-S(2)#3 | 66.58(8) | S(3)-Ga(1)-S(3)#4 | 111.50(13) |

Symmetry transformations used to generate equivalent atoms:

#1 -x+1,-y,z #2 -y+1/2,x-1/2,-z+1/2 #3 y+1/2,-x+1/2,-z+1/2

#4 x-1/2,y-1/2,z-1/2 #5 -x+3/2,-y+1/2,z-1/2

#6 y,-x+1,-z+1 #7 -y+1,x-1,-z+1 #8 y+1/2,-x+1/2,-z+3/2

#9 -y+1/2,x-1/2,-z+3/2 #10 -y+1,x,-z+1 #11 -x+3/2,-y+1/2,z+1/2

#12 x-1/2,y+1/2,z+1/2 #13 -x+1,-y+1,z #14 x+1/2,y+1/2,z+1/2

#15 y+1,-x+1,-z+1 #16 -x+2,-y,z #17 x+1/2,y-1/2,z-1/2

**References**


1. Bruker. Program SAINT. Madison: Bruker AXS Inc. 2012
2. G. Sheldrick, A short history of SHELX, *Acta. Crystlogr. A. Found. Crystlogr.* 2008, **64**, 112-122.
3. O. Dolomanov, A. Blake, N. Champness and M. Schroder, Champness and M. Schroder, OLEX: new software for visualization and analysis of extended crystal structures, *J. Appl. Crystallogr.* 2003, **36**, 1283-1284.
4. P. Kubelka and F. Munk, An Article on Optics of Paint Layers, Z. *Tech. Physical.* 1931, **12**, 593-601.
5. S. Kurtz and T. Perry, A Powder Technique for the Evaluation of Nonlinear Optical Materials, *J. Appl. Phys.* 1968, **39**, 3798-3813.
6. M. Zhang, X, Jiang, L, Zhou and G. Guo, Two phases of $Ga_2S_3$: promising infrared second-order nonlinear optical materials with very high laser induced damage thresholds, *J. Mater. Chem. C* 2013, **1**, 4754-4760.
7. S. Clark, M. Segall, C. Pickard, P. Hasnip, M. Probert, K. Refson and M. Payne, First principles methods using CASTEP, *Z. Krist- Cryst. Mater.* 2005, **220**, 567-570.
8. B. Silvi and A. Savin, Classification of chemical bonds based on topological analysis of electron localization functions, *Nature* 1994, **371**, 683-686.
9. J. Perdew, K. Burke and M. Ernzerhof, Generalized Gradient Approximation Made Simple, *Phys. Rev. Lett.* 1996, **77**, 3865-3868.
10. J. Lin, A. Qteish, M. Payne and V. Heine, Optimized and transferable nonlocal separable ab initio pseudopotentials, *Phys. Rev. B* 1993, **47**, 4174-4180.
11. C. Aversa and J. Sipe, Nonlinear optical susceptibilities of semiconductors: Results with a length-gauge analysis, *Phys. Rev. B* 1995, **52**, 14636-14645.
12. H. Monkhorst, Special points for Brillouin-zone integrations, J. Pack, *Phys. Rev. B* 1976, **13**, 5188-5192.
13. R. He, Z. Lin, M. Lee and C. Chen, Ab initio studies on the mechanism for linear and nonlinear optical effects in $YAl_3(BO_3)_4$, *J. Appl. Phys.* 2011, **109**, 103510.
14. A. Harasaki and K. Kato, New Data on the Nonlinear Optical Constant, Phase-Matching, and Optical Damage of $AgGaS_2$, *JPN. J. Appl. Phys.* 1997, **36**, 700-703.
15. B. Liu, X. Jiang, B. Li, H. Zeng and G. Guo, $Li[LiCs_2Cl][Ga_3S_6]$: A Nanoporous Framework of $GaS_4$ Tetrahedra with Excellent Nonlinear Optical Performance, *Angew. Chem. Int. Ed.* 2020, **59**, 4856-4859.
16. P. Yu, L. Zhou and L. Chen, Noncentrosymmetric inorganic open-framework chalcohalides with strong middle IR SHG and red emission: $Ba_3AGa_5Se_{10}Cl_2$ (A = Cs, Rb, K), *J. Am. Chem. Soc.* 2012, **134**, 2227-2235.
17. Y. Li, P. Liu, L. Hu, L. Chen, H. Lin, L. Zhou and L. Wu, Strong IR NLO Material $Ba_4MGa_4Se_{10}Cl_2$: Highly Improved Laser Damage Threshold via Dual Ion Substitution Synergy, *Adv. Opt. Mater.* 2015, **3**, 957-966.
18. B. Liu, X. Jiang, H. Zeng and G. Guo, $[ABa_2Cl][Ga_4S_8]$ (A = Rb, Cs): Wide-Spectrum Nonlinear Optical Materials Obtained by Polycation-Substitution-Induced Nonlinear Optical (NLO)-Functional Motif Ordering, *J. Am. Chem. Soc.* 2020, **142**, 10641-10645.
19. B. Liu, H. Zeng, X. Jiang, G. Wang, S. Li, L. Xu and G. Guo, $[A_3X][Ga_3PS_8]$ (A = K, Rb; X = Cl, Br): promising IR non-linear optical materials exhibiting concurrently strong second-harmonic

generation and high laser induced damage thresholds, *Chem. Sci.* 2016, **7**, 6273-6277.
20. H. Chen, Y. Li, B. Li, P. Liu, H. Lin, Q. Zhu and X. Wu, Salt-Inclusion Chalcogenide $[Ba_4Cl_2][ZnGa_4S_{10}]$: Rational Design of an IR Nonlinear Optical Material with Superior Comprehensive Performance Derived from $AgGaS_2$, *Chem. Mater.* 2020, **32**, 8012-8019.
21. K. Feng, L. Kang, Z. Lin, J. Yao and Y. Wu, Noncentrosymmetric chalcohalide $NaBa_4Ge_3S_{10}Cl$ with large band gap and IR NLO response, *J. Mater. Chem. C* 2014, **2**, 4590-4596.
22. I. Brown and D. Altermatt, Bond-valence parameters obtained from a systematic analysis of the Inorganic Crystal Structure Database, *Acta Crystallogr. B* 2010, **41**, 244-247.